Remote Sensing of Environment 193 (2017) 216–224

Contents lists available at ScienceDirect

Remote Sensing of Environment

journal homepage: www.elsevier.com/locate/rse

Use of time-series L-band UAVSAR data for the classification of agricultural fields in the San Joaquin Valley

Tracy Whelen, Paul Siqueira *

Department of Electrical and Computer Engineering, University of Massachusetts, Amherst, MA 01003, United States

ARTICLE INFO

Article history:
Received 20 April 2016
Received in revised form 27 February 2017
Accepted 12 March 2017

Keywords:
SAR
Backscatter
Polarimetric decomposition
Time series
Agricultural land cover classification

ABSTRACT

The study of agriculture and agricultural production is an important part of societal planning for allocation of resources and economic forecasting. The prediction of crop output requires collecting accurate crop data throughout the growing season, in locations with a wide range of climatic conditions. Repeat observations from synthetic aperture radar (SAR) have been shown to be a reliable way of gathering frequent crop measurements, even in perpetually cloudy regions.

In this work, repeat coverage of an area in California's San Joaquin Valley, with images taken by NASA's L-band Uninhabited Aerial Vehicle Synthetic Aperture Radar (UAVSAR) system approximately once a month during 2010 and 2012, was used to examine a time-history of backscatter signatures and polarimetric H/A/alpha (Entropy, Anisotropy, and Polarization angle) decomposition values of alfalfa, corn, and winter wheat with the objective of improving classification of individual crops. Distinguishable signatures were observed for all three crops. The signature was dominated by the growth stage and physical structure of the crops during the mature part of the growing season, and by weather events, planting practices, and harvesting procedures during other parts of the year. These data support previous findings that multiple images throughout the year capture the full growth pattern, allowing for more accurate identification of agricultural crops than what can be determined by a single image. The overall accuracies for this time-series classification were 75% using HV-polarized backscatter, 79% using the alpha decomposition, and 83% using the entropy decomposition, which were the three polarizations or decompositions with greatest separability between crops. It is shown that the full-year time series of images builds a more comprehensive model for crop backscatter than previous works.

1. Introduction

Agriculture is critical for economic and societal stability, both for major exporters such as the United States, as well as for many developing nations (FAO, 2013). In order to make accurate estimates for forecasting harvests and crop insurance, crop type and area must be routinely measured throughout the year. If these measurements are done entirely by visits to individual fields, the task rapidly becomes overwhelming in terms of labor and time (Jayne and Rashid, 2010). It also leads to discrepancies when calculating yields or acreage at a continental or global scale, as individual smaller localities may use widely differing methodologies to monitor their fields. This has led to significant research into using remote sensing to gather agricultural data in which individual fields are differentiable. These techniques take measurements throughout the electromagnetic spectrum, including using synthetic aperture radar (SAR) (Becker-Reshef et al., 2010). Because of the wavelengths used in active L- and C-band SAR systems, remote sensing data from these systems are mostly independent of atmospheric conditions. This allows for the reliable collection of data in areas with frequent cloud cover. Additionally, radar provides data about the stem and leaf structure of vegetation, as well as being sensitive to soil roughness and moisture content, making SAR of key interest for agricultural applications (Ulaby et al., 1986).

Increasing numbers of airborne and spaceborne SAR systems have led to increased research being done using only SAR data. Previous work has investigated the role of wavelengths, polarization, polarimetric decompositions, image timing, and data processing routines in differentiating landcover types (Baghdadi et al., 2009; Haldar et al., 2012; Jiao et al., 2014; Tso and Mather, 1999). In areas that are fully vegetated, short SAR wavelengths such as X-band (3 cm) and C-band (6 cm) interact most strongly with the top of the vegetation canopy, whereas long wavelengths such as L-band (20 cm) and P-band (100 cm) are able to penetrate through the vegetation cover, scattering off of lower vegetation structures and the soil. In regions that are not completely covered in vegetation, such as a recently planted field, shorter wavelengths will also scatter off of the soil. Microwave remote sensing of agricultural targets can be successfully achieved by being sensitive to both the fine-

* Corresponding author.
E-mail address: siqueira@umass.edu (P. Siqueira).

http://dx.doi.org/10.1016/j.rse.2017.03.014
0034-4257/

scale structural characteristics of different crop types and growth stages, while at the same time detecting changes in soil moisture and other soil characteristics. For this reason, both L- and C-band have been found to be the most effective wavelengths for agricultural applications (Baronti et al., 1995; Ferrazzoli et al., 1997; Hoekman and Vissers, 2003; Lee et al., 2001).

One of the main areas of agricultural research done with L-band and C-band data has been landcover classification. Some projects have focused on the relatively less complex task of separating crop areas from non-crop areas (Li et al., 2012; Mishra et al., 2011) or identifying one or two major crops (Baghdadi et al., 2009; Chakraborty et al., 2005; Silva et al., 2009), whereas other projects have attempted to identify many unique crops within a geographically limited study area (Hoekman and Vissers, 2003; Mahdian et al., 2013; McNairn et al., 2009). In addition to the classification work done with various combinations of HH, HV, and VV polarizations, classifications have also been made using polarimetric decompositions of fully polarimetric data in traditional classification algorithms alongside, or in place of, HH, HV, and VV (Benz and Pottier, 2001; Hoekman and Vissers, 2003; McNairn et al., 2009), or in classification algorithms based entirely on methods of polarimetric decomposition (Cloude and Pottier, 1997). Common to all of these approaches, through the physical principal of reciprocity, it is assumed that the HV polarized response is the same as the VH polarization (Harrington, 1961; Henderson and Lewis, 1998).

In addition to classification, a small amount of research has looked at the normalized radar cross section given by individual crop types for use in crop identification (Panigrahy et al., 1999; Silva et al., 2009; Tso and Mather, 1999). These studies provide useful data that can improve classification algorithms; however they examine few fields and crop types, a limited time span, and comprise only a handful of studies compared to the number investigating any type of crop classification using SAR data.

The recently launched C-band Sentinel-1 mission, and the upcoming NASA-ISRO SAR (NISAR) and Satélite Argentino de Observación Con Microondas (SAOCOM) L-band missions that are set to launch in the next five years will provide significant amounts of freely available temporal and spatial L- and C-band coverage to make widespread operationalization of SAR data for agricultural purposes feasible (Burns, 2016; Comision Nacional de Actividades Espaciales (CONAE), n.d.; Rosen et al., 2015). Operationalization will require further development of existing classification algorithms and techniques, thus additional data exploration and analysis are needed. In particular, given the short repeat-time of the upcoming satellites, there are opportunities for classification algorithms based on time series spanning multiple seasons.

The expected increase in L- and C-band data that are freely available with high temporal resolution worldwide, combined with previous success at various forms of crop classification and SAR-based measurements, sets the stage for rapidly increasing operationalization of SAR for agricultural purposes. In order to do this successfully, the data must be able to distinguish between a wide range of crops, spread across overlapping seasons, and distributed across many different climatic zones. Full-year coverage can aid in the classification of areas with complex cropping practices, such as the growth of perennials or some fields raising multiple crops per year, as well as allowing for standard off-season field practices to be included in the crop model. The increased temporal availability is important because, through the use of time series, a much more complete annual model can be built for individual crops. This in turn can be used to improve classification, either as a standalone classification algorithm, or as a way to fine-tune the best dates to use with more traditional classification algorithms.

This study focuses on using a full-year time series as a standalone method of classification. It analyzes repeat-observation quad-pol L-band SAR images taken by NASA/JPL's UAVSAR system, of an agricultural area in California's San Joaquin Valley, to test the effectiveness of this method of classification. With near monthly coverage throughout the entire year, this study builds a more detailed annual model of crop backscatter response than what has been developed by previous research. The annual crop models for the three main crops in the study area are used in the time series classification of this region. Expansion of this work to additional crop types and locations will be possible when yearlong coverage by spaceborne SAR systems with even more frequent repeat coverage becomes available within the next few years.

2. Data

This study used imagery from the UAVSAR system, given that it is freely available L-band data, with appropriate technical parameters, and spatial and temporal coverage to be suitable for investigating what can be learned from SAR images of agricultural areas. UAVSAR is a fully polarimetric L-band SAR system with a bandwidth of 80 MHz, single-look-complex data (SLC) pixel spacing of 0.6 m × 1.6 m, and a swath width of approximately 20 km spanning an incidence angle range of 25°–65°, which has been operational since 2009 (Chapman et al., 2011). This system has been used to collect data for a diverse range of projects on multiple continents, studying a range of geophysical hazards, sea ice, and characterizing forested and agricultural vegetation (Brekke et al., 2014; Dickinson et al., 2013; Donnellan et al., 2014; Jones et al., 2011; Mahdian et al., 2013). The images used in this study were originally collected as part of an on-going campaign to monitor the levees in the Sacramento-San Joaquin Delta region in central California.

The data set analyzed here was selected from all UAVSAR data, based on its ability to meet the following criteria: 1.) it needed to have repeat coverage of mainly agricultural land, with repeat coverage comprising of at least six images from a single year, with multiple images during the main growing season, and 2.) the majority of the fields needed to be growing one of a handful of major crops, such as corn, rice, wheat, etc., with enough pixels for both training and classification of each crop. Additionally these criteria all had to be met for multiple years in the same area, with the same UAVSAR image geometry, so that comparisons could be made across seasons. A full year of data was used in order to investigate classification of crops that did not follow the same crop calendars, and to investigate the presence of standard off-season patterns that could be indirectly used in crop classification. A full year of data also allowed the radar data to indicate the times with best separability, rather than the authors guessing from a limited selection of image dates.

Since the majority of UAVSAR images, especially over multiple years in the same location, have been taken in California, and since the San Joaquin Valley of California is a major agricultural area, the first step in data selection was to find all of the UAVSAR images that overlapped with San Joaquin Valley agricultural areas. Once regions had been narrowed down by selecting for the most number of images and images during the growing season, the United States Department of Agriculture's (USDA) Cropland Data Layer (CDL) was used to determine optimal crop areas (United States Department of Agriculture National Agricultural Statistics Service (USDA NASS), 2009–2012). The CDL was also used as ground truth, due to the use of historical images preventing ground truth from being collected by the authors at the same time as the images were collected. While not 100% accurate, the 2010 California layer has statewide accuracies of 77%–91% for the three crops examined in this study (USDA NASS, 2011). A visual inspection of the CDL suggests that it mainly has error problems at the edges of fields, or occasionally labels a field as being a mixture of two crops. The authors feel that the error rates for these three crops are low enough, and close enough to each other, that it is safe to assume that a field primarily classified as a crop most likely is that same crop, even if a few edge pixels disagree. A significant portion of California's agriculture is comprised of fruits and vegetables, meaning that in any given area there is likely to be two to four main crops interspersed with a variety of other smaller crops. This region was chosen because its main crops were all field crops, as opposed to many parts of California where there might be

one or two major field crops, vineyards, a major fruit or nut tree crop, and a dozen different assorted field and vegetable crops that each have too few pixels for the training and testing of a classification algorithm. A greater number of major field crops would have been ideal, but this was not possible with other data acquisition constraints.

The final study area was a region roughly 10 km × 23 km located on the western side of Stockton, CA in San Joaquin County. It was comprised of nineteen SAR images, ten taken in 2010 and nine taken in 2012. There was roughly one image per month, skipping December and the occasional other month. Most of the study area is agricultural land, with the main crops consisting of alfalfa, corn, and winter wheat (USDA NASS, 2009–2012). These three crops are globally important food crops for humans (corn and wheat) and livestock (corn and alfalfa), representing a mixture of seasonal growing patterns, with alfalfa being a perennial, corn planted in the spring and harvested in the fall, and winter wheat planted in the fall and then grown over winter to be harvested the next summer. A portion of the city of Stockton, CA is on the northeastern edge of the study area, and a portion of the Clifton Court Forebay artificial reservoir on the southwestern edge (Fig. 1).

3. Data processing

The analysis consisted of two main steps. First, per-field statistics were calculated from each image for a set of fields for each crop. The statistics from each scene date were then used to create a model of the average backscatter response over the course of a calendar year. Second, an error metric derived from these models was used to classify a time series of images. This classification method classifies one crop from another, which can be viewed as the final step of a classification such as those used in the production of the CDL, or the Canadian equivalent produced by Agriculture and Agri-Food Canada that first classify crops from non-crops, and then second, differentiates between individual crops (Boryan et al., 2011; Fisette et al., 2013).

In order to calculate the average field backscatter response, twenty-five fields each of alfalfa, corn, and winter wheat were marked for 2010. The process of field plot marking comprised two steps; first selecting the appropriate crop type from the CDL data, and second selecting twenty-five fields that were within the field boundaries visible in the SAR images. The pixels of these twenty-five training fields were excluded from the eventual classification. Pixels were selected that were completely surrounded by that same crop, and then the resulting regions were further trimmed and selected. In order to get sufficient in-field statistics, plots less than eight hectares in size were excluded. Almost all of the fields in the study area were over six hectares in size, and most of them were ten to thirty hectares. This also helped to remove areas with obvious confusion in the CDL classification. The selected final field plots were chosen to be distributed throughout the study area and to be between eight and twenty-five hectares once their boundaries had been made to fit within the fields visible in the SAR images. An example of the field marking process is shown in Fig. 2.

Before the images could have useful statistics extracted from them, or be otherwise analyzed, they needed to be geocoded and all units converted to Normalized Radar Cross Section (NRCS; σ° dB m^2/m^2). The images used for the project were the 3 × 3 multilooked version produced by the Alaska Satellite Facility (ASF), resulting in a pixel size of 5 m × 5 m. No additional speckle filters were used because the images had already been multilooked, and the time series analysis of images consists of the statistical behavior of thousands of pixels, and hence, the effect of speckle is effectively non-existent. The geocoding was done with the MapReady software created by ASF (Alaska Satellite Facility, 2012). A full UAVSAR image has an incidence angle range of 25°–65°; however the data set region used for this agricultural study spans approximately 32°–51°. This incidence angle range is small enough such that the effect of the scattering law (a proportional dependence of σ° on $\cos^n\Theta$) is expected to be minimal.

The six layers under investigation for each image date were the backscatter (HH, HV, and VV) and the H/A/α polarimetric decomposition (entropy, anisotropy, and alpha). For each of these six layers, the mean value for each field was calculated. Previous works have investigated the mean backscatter response of individual crops for a variety of reasons (Blaes et al., 2005; Brown et al., 1992; Panigrahy et al., 1999; Silva et al., 2009; Torbick et al., 2011). To perform a cross-field statistical characterization of each crop across a given layer, the mean and standard deviation of all of the field means were calculated for every crop – layer class (for example, the HV-polarized response for corn). These were then used to calculate an error metric that was used as the basis of the classification algorithm. For each crop type, this metric

Fig. 1. Study area location. The blue rectangle marks the boundaries of the study area. Imagery is from June 2014, as compiled by ESRI from a variety of sources depending on zoom level (ESRI, 2012).

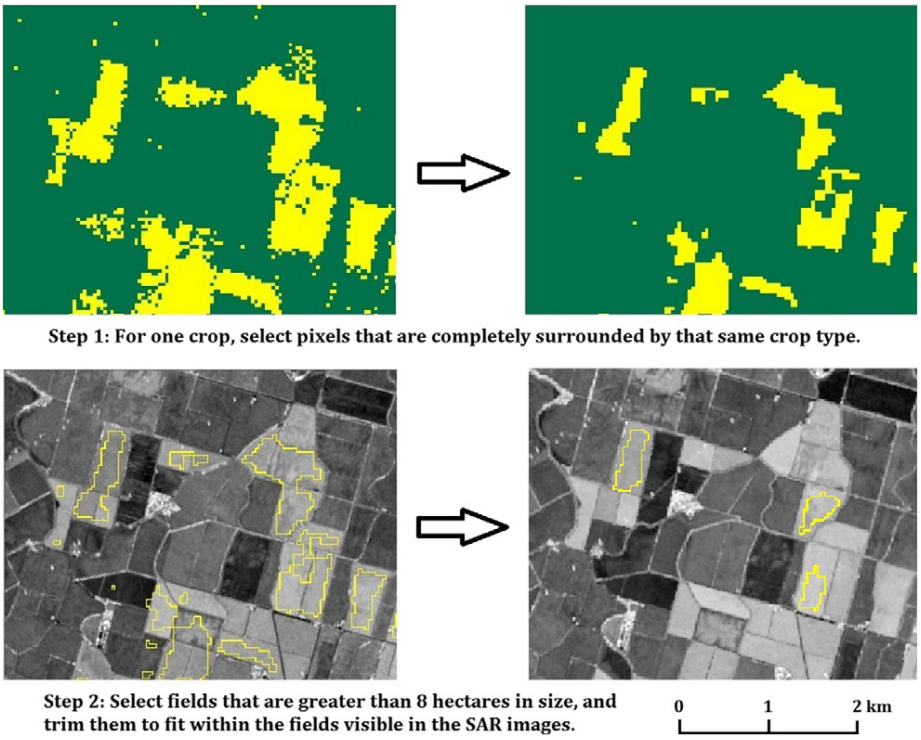

Fig. 2. Field marking procedure. The two steps consisted of selecting the appropriate crop type from the CDL data, and then selecting twenty-five fields, and making sure they fit within the fields visible in the SAR images.

was determined by

$$err_{class} = \sum_{N} \frac{|\sigma^{\circ}_{obs}(n) - \sigma^{\circ}_{class}(n)|}{std(\sigma^{\circ}_{class}(n))} \quad (1)$$

where $\sigma^{\circ}_{obs}(n)$ and $\sigma^{\circ}_{class}(n)$ are the observed (per-pixel) and class-related mean NRCS as a function of the observation number, n (equivalently an observation date), and $std(\sigma^{\circ}_{class}(n))$ is the standard deviation of the field mean NRCS values for each layer, also as a function of the observation number. Normalizing the error metric in this way serves two purposes: 1.) it creates a unitless, probability-based measure of the error, and 2.) it takes into account the variations that occur at specific times of the year. For instance, during the planting and harvesting seasons, where field-to-field variations are expected to dominate the overall error, normalization by the standard deviation reduces the effect of these variations on the overall error metric given in Eq. (1). In a crop like alfalfa with multiple harvestings across the year, while the difference between observed and class NRCS might be larger, the standard deviation would also be expected to be larger, and thus would account for this time variation in backscatter response for each crop-type. The result of this metric is the error observed assuming that a particular pixel belongs to a given crop class (e.g. corn, wheat, etc.). During the classification step, the pixel is assigned the classification with the minimum error.

The model values used in this classification were based on the 2010 field plots, but the model was used to classify both the 2010 and 2012 time series so as to compare consistency between years. The model should give a generic picture of crop behavior, so with no major climatic variations between the two years the 2010 model should be reasonable for use with 2012 images. For the 2012 classification, the 2010 data were interpolated using a cubic spline interpolation to estimate backscatter, alpha, and entropy values at the same dates as each of the 2012 images. The training pixels were removed from the 2010 data when classifying and calculating classification accuracies, so that the training pixels were completely independent from pixels being classified. As the 2010 model was used for 2012, there was no need to remove any training pixels from the 2012 data set.

Of the three principal polarizations (HH, HV, and VV), when graphing the average power over a field as a function of time, the HV-polarized response was better separated compared to the time series derived from HH- and VV- polarized average power. A similar analysis was performed using the three components of the polarimetric decomposition (H/A/α; entropy, anisotropy, and alpha). Of the three decompositions, anisotropy did not have a clear distinction between crops, and alpha and entropy both had very clear patterns that were equally distinct. Because of these patterns, the HV-polarized backscatter, and polarimetric decomposition variables of alpha and entropy were chosen to test the classification algorithm. Only pixels that were originally classified as alfalfa, corn, or winter wheat in the CDL were used to test the classification algorithm.

4. Results

The main points from this study consist of the following observations. First, that there are clearly visible seasonal patterns of SAR backscatter values which seem to be connected to plant type and phenology. This was true for both backscatter and decomposition images. Second, the error metric model was able to produce classifications with overall accuracies ranging from 75%–83% for both the 2010 and 2012 images. This is significant because data from the 2012 observations were not used in the training of the classifier.

The three studied crop types, alfalfa, corn, and winter wheat, showed a consistent pattern across all three polarization means. The corn had its lowest values in the spring (April and May), highest values in the summer and early fall (July through October), and intermediate values during the winter months. In contrast, alfalfa and winter wheat had their highest values in the spring and their lowest values during the summer. If crops are compared to where they are along the growing season (as opposed to calendar year) there becomes one pattern for all three crops, with high values at peak vegetation just before harvest, and low

values during the offseason, consistent with scattering models of short vegetation (Macelloni et al., 2001; McNairn et al., 2009). The crop averages from the HV-polarized backscatter show these patterns most clearly, as can be seen in Fig. 3. The patterns were also visible in the HH- and VV- polarized averages of backscatter for the crops; however instead of the 10–15 dB average separation between corn and the other two crops in HV, there was only 5–8 dB of separation for HH and VV. For both HH- and VV-polarized backscatter, the field means fell in the range of −13 to −22 dB, as compared to the range of −20 to −35 dB seen with HV. The crop calendar for these crops in this part of California is shown in Fig. 4. All crops fit within the range of backscatter values typical for shrubs and short vegetation using L-band between 30°–50° incidence angle with all three polarizations (Ulaby and Dobson, 1989).

These seasonal patterns were even clearer when analyzing entropy and alpha of the H/A/α decomposition. Entropy and anisotropy are measured on a scale from zero to one, whereas the alpha angle ranges from 0° to 90° (Cloude and Pottier, 1997), and are used to characterize properties of the target scattering mechanisms. When analyzing the alpha layer, alfalfa had high values for most of the year, with a mean around 40°–45°, indicating a high degree of random scattering from a volume (i.e. alpha is an indication of the preferred polarization state of a target, with 45° often indicating a target with no preferred polarization). Analysis of the entropy images resulted in patterns very like those of the alpha data. The similarities between the alpha and entropy patterns can be seen in Fig. 5. The anisotropy layer provided minimal distinguishing information about the crops.

Using the time series classification approach described in Eq. (1), the classification of the 2010 images (Fig. 6) had overall accuracies of 75% for HV-polarized backscatter, 79% for alpha, and 83% for entropy for the polarimetric decomposition parameters. The 2012 classification, based on the 2010 crop models, had equally good results, with overall accuracies of 83% for HV, 82% for alpha, and 82% for entropy. Almost all user's and producer's accuracies for individual crops for both classifications were over 70%, suggesting that no one crop result was dominating the overall accuracy results. Most of the misclassified pixels were in regions where the CDL used as ground truth had difficulties with classification, such as at field edges or fields that the CDL had classified as a combination of multiple interwoven crops. These results are summarized in Table 1 below. Further analysis of combined HV, alpha, and entropy layers to refine the classification showed minimal improvement, indicating that the majority of information content in the polarization signature could be captured with just one of these layers.

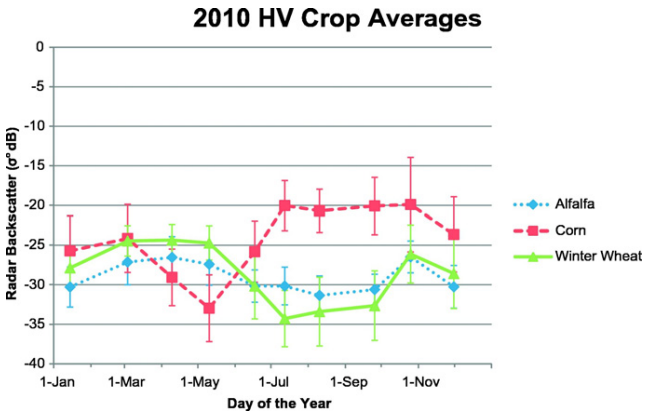

Fig. 3. HV-polarized crop averages for the 2010 growing year. Each point on a line shows the mean of the field averages from one image for that crop-year-polarization combination. Error bars show one standard deviation for that population of twenty-five field means determined on the day of observation.

5. Discussion

These results show patterns related to plant structure and growing behavior, which allow for moderately accurate classification. Corn has larger leaves and stems that are more widely spaced and randomly oriented than the dense structure of alfalfa and winter wheat. Examples of each crop can be seen in Fig. 7. It is reasonable to expect that as tightly growing, small structured crops, alfalfa and winter wheat would have less seasonal variation in backscatter value as compared to corn, which grows from seedlings to tall plants with large leaves over the course of a season. This is visible in the data in that the alfalfa and winter wheat fields cover a smaller range of σ° values across the course of a year than the corn fields. For example, depending on year and polarization, an alfalfa field normally changes 4–8 dB between the highest and lowest values in a year. In contrast, a corn field under those same circumstances might change 10–20 dB throughout the year. Additionally, the most rapid changes in values for the corn fields are during the main growing season (May–July) and harvest (late fall) (USDA NASS, 2010). This corresponds to past work that has found that broad-leafed crops with higher biomass, (e.g. corn, sunflowers, and sorghum) have higher HV-polarized backscatter values than narrow-leafed low biomass crops (e.g. alfalfa and wheat) (Macelloni et al., 2001).

The alpha and entropy values also show distinct structure-related scattering patterns for each crop. Alfalfa's consistent alpha values around 40°–45°, combined with mid-range entropy values suggest that it can be modeled as randomly oriented dipoles for studying scattering mechanisms (Lee and Pottier, 2009). Corn and winter wheat both support a correlation between increasing entropy as the crop matures, with peak entropy values following the crop calendar. This is similar to the work of McNairn et al. (2009), who found a correlation between increasing biomass and an increase in the randomness of the scattering for corn. In addition, the shift from low alpha and entropy to high alpha and entropy polarimetric decomposition values across the growing season for corn and winter wheat suggests that soil has a large influence on the off-season scattering, based on the different zones of the H-alpha plane (Cloude and Pottier, 1997). In contrast, alfalfa as a perennial shows little variation of alpha and entropy across the year, as expected.

A source of noise for some of the images is extra soil moisture due to recent rain. In the two days preceding the January 14, 2010 image, 1.68 cm of rain was recorded, and 1.47 cm of rain was measured on the day of the March 3, 2010 image on top of 0.61 cm that had fallen the day before. In addition, the study area received 3.00 cm of rain in the two days preceding the October 25, 2010 image (NOAA/NWS, 2015). The official record measures rain in inches; the centimeter equivalents are given here for consistency with the metric system. Rain has the effect of increasing the soil conductivity for short periods of time (approximately one day), and hence increasing the reflectivity, of the soil. When the soil is bare, as in times before the crop is growing, such changes have a strong contribution to the overall scattering from the crop region. As the vegetation grows, the scattering response from the ground surface is attenuated by the vegetation layer. A notable exception occurs when the soil is very wet, or even inundated, as is the case with rice, where the double-bounce return from the vegetation-soil interface can dominate the signal return. Here however, the returns are dominated by the simpler direct vegetation and soil returns, and so for a dense times series (e.g. monthly observations) these effects were not strongly pronounced. These high precipitation dates could influence the field averages for those days, slightly adjusting the overall model. The times of year when this would have the biggest influence on crop models would be at either end of a growing season, such as when one crop has just been harvested, whereas the field next to it is still full of vegetation. Models based on data from a wide geographic area over multiple years should limit the influence of any single rain event.

The classification results presented here show promise for using time series to classify individual crops. By spanning the entire year,

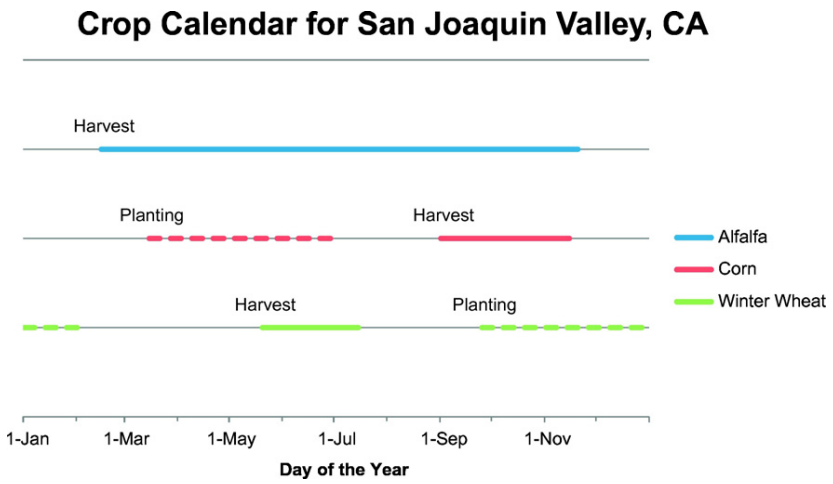

Fig. 4. Crop calendar for alfalfa, corn, and winter wheat. Dashed lines show the planting time and solid lines show the harvest time. Alfalfa as a perennial crop does not have a yearly planting time. Note that winter wheat is planted in the fall and winter, and is harvested during the early summer of the next calendar year (USDA NASS, 2010).

the time series is able to capture patterns that are dependent on the state of growth and off-season field behavior. With the upcoming satellite missions that deliver data over multiple years, a more robust model could be built using data from multiple calendar years, so that climate-related temporal shifts in the crop calendar for an individual year could be accounted for by allowing for constrained shifts in the SAR-data time series. With the current single-year model, the greatest separation between crops happens in the late spring (May) and then late summer into early fall (mid-July through early October). However in a region with different crops and/or growing seasons the most important times for image gathering might shift. Even over this same region, a year with an extremely abnormal crop calendar, such as much later planting due to a very long winter could have difficulties being classified since plant growth would be offset from the model data. A multi-year model would account for this type of variation, and give more robust guidance on the most important times of year during which to capture images. The current model and trial data leads to classification accuracies ranging from 75% to 83%, depending on the polarization or decomposition under classification. Since most of the misidentified pixels were along the edges of fields, it suggests that more precise ground truth data or classification at the field level could greatly improve the classification accuracy.

When examining entire fields that had been misclassified, there were sixty-one fields in 2010 that were misclassified in the HV, alpha, and/or entropy data. These fields were examined for how they had been misclassified and what crops they were planted with in the years on either side (2009 and 2011) according to the CDL (USDA NASS, 2009–2012). Forty-nine of the sixty-one fields were misclassified in at least the HV data. The graphed crop averages across time (Figs. 3 and 5 in the text) suggest that the proposed method in HV might have a harder time differentiating between crops because there is less separation between the crop averages, especially in the springtime. It had the most difficulty distinguishing between alfalfa and winter wheat, as is shown by the majority of misclassified fields that were consistently

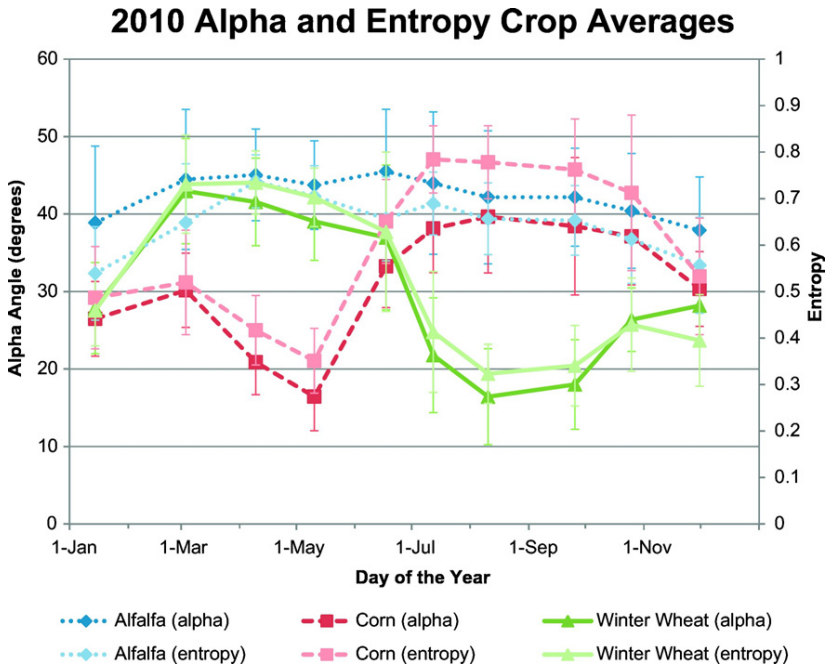

Fig. 5. 2010 alpha (left vertical axis) and entropy (right vertical axis) crop averages. This graph shows the average mean for the twenty-five fields of each crop type for both alpha and entropy. Error bars show one standard deviation for the population of twenty-five field means.

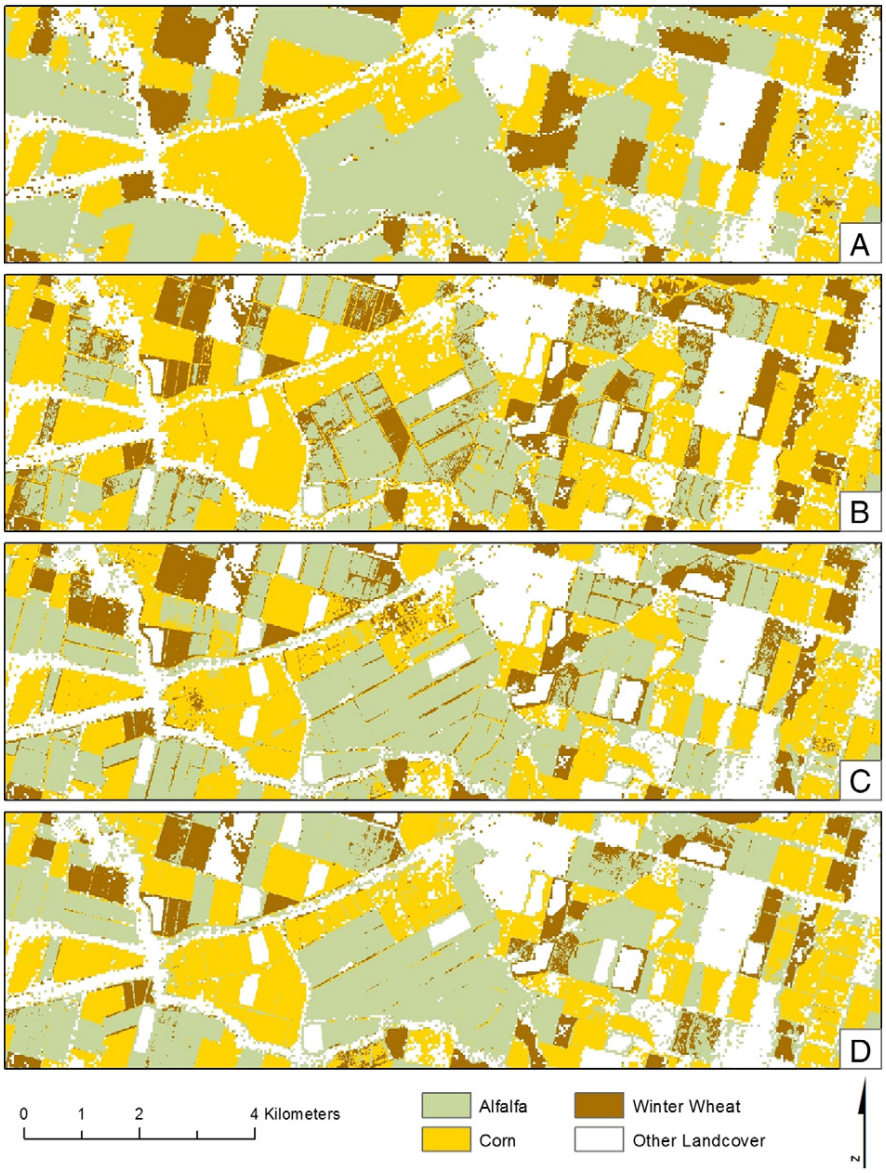

Fig. 6. Classification results using the time series error metric given by Eq. (1) for the 2010 Cropland Data Layer (A: CDL) and (B) the 2010 HV-polarized backscatter, (C) the 2010 alpha classification, and (D) the 2010 entropy classification. The field regions missing from the classifications are areas of training pixels. Similar results and accuracies have been noted when using the 2010 time series-derived classifier on UAVSAR data collected in 2012.

planted with alfalfa being mistaken for winter wheat. This was also true for fields that were planted with alfalfa in 2009 and 2010, even if they grew a different crop in 2011. For the five fields that grew winter wheat in 2009 before switching to alfalfa for 2010 the crop calendars show a mid-project crop rotation could be cause of the confusion, or it could be more general confusion between alfalfa and winter wheat in

Table 1
Summary of classification results.[c]

Crop	Year	HV classification		Alpha classification		Entropy classification		CDL state-wide	
		User's[a]	Producer's[b]	User's	Producer's	User's	Producer's	User's	Producer's
Alfalfa	2010	96%	53%	80%	77%	81%	84%	83%	91%
Corn	2010	80%	96%	88%	83%	90%	87%	84%	90%
Winter wheat	2010	44%	75%	56%	74%	68%	69%	77%	78%
Alfalfa	2012	88%	79%	84%	81%	87%	79%	92%	94%
Corn	2012	85%	95%	82%	84%	80%	80%	89%	89%
Winter wheat	2012	61%	63%	76%	80%	73%	86%	76%	73%

[a] User's accuracy is the fraction of correctly classified pixels out of all pixels classified as that category.
[b] Producer's accuracy is fraction of correctly classified pixels out of all pixels in that ground truth category.
[c] An example of user's accuracy is the number of pixels the ground truth and classification both label as corn divided by the total number of pixels classified as corn, whereas the producer's example would be those same correctly classified as corn pixels divided by the total number of pixels labeled as corn in the CDL dataset.

Fig. 7. Crop examples for alfalfa, corn, and winter wheat. Here are pictures of each crop well into the growing season (left to right): alfalfa, winter wheat, and corn. All images courtesy of Google Images.

HV. The crop calendars suggested that mid-project crop rotations were not a likely reason for most of the misclassification.

The CDL data set that was used here was the best available ground truth; however, at a statewide level, it has classification accuracy ranging between 70%–95% for the three crops in the two years, leaving plenty of room for improvement. Six of the aforementioned misclassified fields were either classified as a mixture of two crops by the CDL, or had very consistent classifications across HV, alpha, and entropy despite that classification differing from the CDL. Similarly there were misclassified fields that the CDL had stated were a mixture of one of the study crops and some other non-study crop. While this project's classification method might have correctly identified the entire field, due to the CDL's faulty classification it was only tested on the part of the field correctly identified by the CDL. These situations show that an improved CDL or other ground truth could have improved the results of this study. In order to improve classification accuracy, potentially full-year L-band SAR data could be incorporated into the creation of the CDL as a complement to the optical imagery currently in use. There is precedence for this, as the Canadian equivalent to the CDL, the Annual Crop Inventory produced by Agriculture and Agri-Food Canada, uses Radarsat-2 data in addition to a variety of optical sources to produce a product with similar accuracy to the CDL (Fisette et al., 2013).That project has also made note of the challenges of accurately classifying a diverse range of crops when imagery is expensive and SAR data has limited temporal availability, meaning that it too could be improved by upcoming new SAR satellites.

6. Conclusion

This paper presents a multi-year, multi-season analysis of airborne SAR data over agricultural fields in central California's San Joaquin Valley. It is noted that the dense time series of observations (approximately one observation per month) provided signatures of the crops during their growing season that can be used as a signature for classification. The multiple images throughout the year allow for matching of entire growing patterns, as well as allowing algorithms to utilize data for specific seasons and crop growth stages for further analysis. As algorithms mature, this type of information will be useful for improved classification of individual crop types, as well as mid-season crop yield and health measurements.

The analysis presented here serves as a predecessor study for the NISAR mission which will make such measurements (albeit at a lower resolution) throughout the year. It is expected that the resolution-related deficiencies of NISAR will be compensated by the increase in images per year, and in geographic distribution. A twelve-day repeat period would lead to thirty images per year, as compared to the nine or ten used in this study, which would give far more sample points for modeling crop behavior and classifying crops. Hence, this approach could form the cornerstone for the automatic identification of crop types based on a dense times series of satellite SAR data.

Acknowledgements

This work was supported by NASA Headquarters under a grant from NASA's Terrestrial Ecology program for studying spaceborne estimation of vegetation structure (NNX09AI18G) and a NASA grant (NNX12AO23G) for supporting the NISAR mission (formerly known as DESDynI). The authors would also like to acknowledge NASA's UAVSAR program for collecting the airborne L-band SAR data used in this analysis.

References

Alaska Satellite Facility, 2012. MapReady [Software]. Available from. https://www.asf.alaska.edu/data-tools/mapready/.

Baghdadi, N., Boyer, N., Todoroff, P., El Hajj, M., Begue, A., 2009. Potential of SAR sensors TerraSAR-X, ASAR/ENVISAT and PALSAR/ALOS for monitoring sugarcane crops on Reunion Island. Remote Sens. Environ. 113 (8):1724–1738. http://dx.doi.org/10.1016/j.rse.2009.04.005.

Baronti, S., Del Frate, F., Ferrazzoli, P., Paloscia, S., Pampaloni, P., Schiavon, G., 1995. SAR polarimetric features of agricultural areas. Int. J. Remote Sens. 16 (14), 2639–2656.

Becker-Reshef, I., Justice, C.O., Sullivan, M., Vermote, E., Tucker, C., Anyamba, A., Small, J., Pak, E., Masuoka, E., Schmaltz, J., Hansen, M., Pittman, K., Birkett, C., Williams, D., Reynolds, C., Doorn, B., 2010. Monitoring global croplands with coarse resolution Earth observations: the Global Agriculture Monitoring (GLAM) Project. Remote Sens. 2 (6):1589–1609. http://dx.doi.org/10.3390/rs2061589.

Benz, U., Pottier, E., 2001. Object based analysis of polarimetric SAR data in alpha-entropy-anisotropy decomposition using fuzzy classification by eCognition. Presented at the Geoscience and Remote Sensing Symposium, 2001 IGARSS'01. 3. IEEE, Sydney, Australia :pp. 1427–1429 Retrieved from. http://www.ecognition.com/sites/default/files/386_ucbenz_igarss2001_2.pdf.

Blaes, X., Vanhalle, L., Defourny, P., 2005. Efficiency of crop identification based on optical and SAR image time series. Remote Sens. Environ. 96:352–365. http://dx.doi.org/10.1016/j.rse.2005.03.010.

Boryan, C.G., Yang, Z., Mueller, R., Craig, M., 2011. Monitoring US agriculture: the US Department of Agriculture, National Agricultural Statistics Service, Cropland Data Layer Program. Geocarto Int. 26:341–358. http://dx.doi.org/10.1080/10106049.2011.562309.

Brekke, C., Holt, B., Jones, C., Skrunes, S., 2014. Discrimination of oil spills from newly formed sea ice by synthetic aperture radar. Remote Sens. Environ. 145:1–14. http://dx.doi.org/10.1016/j.rse.2014.01.015.

Brown, R.J., Manore, M.J., Poirier, S., 1992. Correlations between X-, C-, and L-band imagery within an agricultural environment. Int. J. Remote Sens. 13, 1645–1661.

Burns, P., 2016, February 2. First Ever UK Digital Crop Map From Satellite Data. Retrieved from. http://www.ceh.ac.uk/news-and-media/news/first-ever-uk-digital-crop-map-satellite-data.

Chakraborty, M., Manjunath, K.R., Panigrahy, S., Kundu, N., Parihar, J.S., 2005. Rice crop parameter retrieval using multi-temporal, multi-incidence angle Radarsat SAR data. ISPRS J. Photogramm. Remote Sens. 59 (5):310–322. http://dx.doi.org/10.1016/j.isprsjprs.2005.05.001.

Chapman, B., Hensley, S., Lou, Y., 2011. The JPL UAVSAR. ASF News & Notes. 7(1) Retrieved from. https://www.asf.alaska.edu/news-notes/7-1/jpl-uavsar/.

Cloude, S.R., Pottier, E., 1997. An entropy based classification scheme for land applications of polarimetric SAR. IEEE Trans. Geosci. Remote Sens. 35 (1), 68–78.

Comision Nacional de Actividades Espaciales (CONAE). (n.d.). SAOCOM: Introduction [Governmental Page]. Retrieved February 24, 2016, from http://www.conae.gov.ar/index.php/english/satellite-missions/saocom/introduction.

Dickinson, C., Siqueira, P., Clewley, D., Lucas, R., 2013. Classification of forest composition using polarimetric decomposition in multiple landscapes. Remote Sens. Environ. 131:206–214. http://dx.doi.org/10.1016/j.rse.2012.12.013.

Donnellan, A., Parker, J., Hensley, S., Pierce, M., Wang, J., Rundle, J., 2014. UAVSAR observations of triggered slip on the Imperial, Superstition Hills, and East Elmore Ranch Faults associated with the 2010 M 7.2 El Mayor-Cucapah earthquake. Geochem. Geophys. Geosyst. 15:815–829. http://dx.doi.org/10.1002/2013GC005120.

Environmental Systems Resource Institute (ESRI), 2012. ArcMap 10.1. ESRI, Redlands, CA (2012).
Ferrazzoli, P., Paloscia, S., Pampaloni, P., Schiavon, G., Sigismondi, S., Solimini, D., 1997. The potential of multifrequency polarimetric SAR in assessing agricultural and arboreous biomass. IEEE Trans. Geosci. Remote Sens. 35 (1):5–17. http://dx.doi.org/10.1109/36.551929.
Fisette, T., Rollin, P., Aly, Z., Campbell, L., Daneshfar, B., Filyer, P., Smith, A., Davidson, A., Shang, J., Jarvis, I., 2013. AAFC annual crop inventory. Agro-Geoinformatics (Agro-Geoinformatics), 2013 Second International Conference on. IEEE, Fairfax, VA: pp. 270–274 http://dx.doi.org/10.1109/Argo-Geoinformatics.2013.6621920.
Food and Agriculture Organization of the United Nations (FAO), 2013. FAO Statistical Yearbook 2013: World Food and Agriculture. Food and Agriculture Organization of the United Nations (FAO), Rome Retrieved from. http://issuu.com/faooftheun/docs/syb2013issuu.
Haldar, D., Das, A., Mohan, S., Pal, O., Hooda, R.S., Chakraborty, M., 2012. Assessment of L-band SAR data at different polarization combinations for crop and other landuse classification. Prog. Electromagn. Res. B 36, 303–321.
Harrington, R.F., 1961. Time-harmonic electromagnetic fields. McGraw-Hill Electrical and Electronic Engineering Series. McGraw-Hill Publishing Company, New York, NY.
Henderson, F.M., Lewis, A.J., 1998. Principles and applications of imaging radar. Manual of Remote Sensing, third ed. John Wiley & Sons, New York, NY.
Hoekman, D.H., Vissers, M.A.M., 2003. A new polarimetric classification approach evaluated for agricultural crops. IEEE Trans. Geosci. Remote Sens. 41 (12):2881–2889. http://dx.doi.org/10.1109/TGRS.2003.817795.
Jayne, T.S., Rashid, S., 2010. The value of accurate crop production forecasts. Presented at the Fourth African Agricultural Markets Program (AAMP) Policy Symposium, Lilongwe, Malawi Retrieved from. http://ageconsearch.umn.edu/bitstream/97032/2/idwp108.pdf.
Jiao, X., Kovacs, J.M., Shang, J., McNairn, H., Walters, D., Ma, B., Geng, X., 2014. Object-oriented crop mapping and monitoring using multi-temporal polarimetric RADARSAT-2 data. ISPRS J. Photogramm. Remote Sens. 96:38–46. http://dx.doi.org/10.1016/j.isprsjprs.2014.06.014.
Jones, C., Bawden, G., Deverel, S., Dudas, J., Hensley, S., 2011. Characterizing land surface change and levee stability in the Sacramento-San Joaquin Delta using UAVSAR radar imagery. Geoscience and Remote Sensing Symposium (IGARSS), 2011 IEEE International. IEEE, Vancouver, BC, Canada:pp. 1638–1641 http://dx.doi.org/10.1109/IGARSS.2011.6049546.
Lee, J.-S., Pottier, E., 2009. Polarimetric Radar Imaging: From Basics to Applications. CRC Press, Taylor & Francis Group, Boca Raton, FL.
Lee, J.-S., Grunes, M.R., Pottier, E., 2001. Quantitative comparison of classification capability: fully polarimetric versus dual and single-polarization SAR. IEEE Trans. Geosci. Remote Sens. 39 (11):2343–2351. http://dx.doi.org/10.1109/36.964970.
Li, G., Lu, D., Moran, E., Dutra, L., Batistella, M., 2012. A comparative analysis of ALOS PALSAR L-band and RADARSAT-2 C-band data for land-cover classification in a tropical moist region. ISPRS J. Photogramm. Remote Sens. 70:26–38. http://dx.doi.org/10.1016/j.isprsjprs.2012.03.010.
Macelloni, G., Paloscia, S., Pampaloni, P., Marliani, F., Gai, M., 2001. The relationship between the backscattering coefficient and the biomass of narrow and broad leaf crops. IEEE Trans. Geosci. Remote Sens. 39 (4):873–884. http://dx.doi.org/10.1109/36.917914.
Mahdian, M., Homayouni, S., Fazel, M.A., Mohammadimanesh, F., 2013. Agricultural land classification based on statistical analysis of full polarimetric SAR data. ISPRS-Int. Arch. Photogramm. Remote Sens. Spat. Inf. Sci. 1:257–261. http://dx.doi.org/10.5194/isprsarchives-XL-1-W3-257-2013.
McNairn, H., Shang, J., Jiao, X., Champagne, C., 2009. The contribution of ALOS PALSAR multipolarization and polarimetric data to crop classification. IEEE Trans. Geosci. Remote Sens. 47 (12):3981–3992. http://dx.doi.org/10.1109/TGRS.2009.2026052.
Mishra, P., Singh, D., Yamaguchi, Y., 2011. Land cover classification of PALSAR images by knowledge based decision tree classifier and supervised classifiers based on SAR observables. Prog. Electromagn. Res. B 30, 47–70.
National Oceanic and Atmospheric Administration, National Weather Service (NOAA-NWS), 2015. NOWData – NOAA Online Weather Data [Governmental Page]. Sacramento, CA, National Weather Service Forecast Office Retrieved August 17, 2015, from. http://www.weather.gov/climate/xmacis.php?wfo=sto.
Panigrahy, S., Manjunath, K.R., Chakraborty, M., Kundu, N., Parihar, J.S., 1999. Evaluation of RADARSAT standard beam data for identification of potato and rice crops in India. ISPRS J. Photogramm. Remote Sens. 54 (4):254–262. http://dx.doi.org/10.1016/S0924-2716(99)00020-9.
Rosen, P.A., Hensley, S., Shaffer, S., Veilleux, L., Chakraborty, M., Misra, T., Bhan, R., Raju Sagi, V., Satish, R., 2015. The NASA-ISRO SAR mission - an international space partnership for science and societal benefit. Radar Conference (RadarCon), 2015 IEEE. IEEE, Arlington, VA:pp. 1610–1613 http://dx.doi.org/10.1109/RADAR.2015.7131255.
Silva, W.F., Rudorff, B.F.T., Formaggio, A.R., Paradella, W.R., Mura, J.C., 2009. Discrimination of agricultural crops in a tropical semi-arid region of Brazil based on L-band polarimetric airborne SAR data. ISPRS J. Photogramm. Remote Sens. 64 (5):458–463. http://dx.doi.org/10.1016/j.isprsjprs.2008.07.005.
Torbick, N., Salas, W.A., Hagen, S., Xiao, X., 2011. Monitoring rice agriculture in the Sacramento Valley, USA with multitemporal PALSAR and MODIS imagery. IEEE J. Sel. Top. Appl. Earth Obs. Remote Sens. 4:451–457. http://dx.doi.org/10.1109/JSTARS.2010.2091493.
Tso, B., Mather, P.M., 1999. Crop discrimination using multi-temporal SAR imagery. Int. J. Remote Sens. 20 (12):2443–2460. http://dx.doi.org/10.1080/014311699212119.
Ulaby, F.T., Dobson, M.C., 1989. Handbook of Radar Scattering Statistics for Terrain. Artech House, Inc., Norwood, MA.
Ulaby, F.T., Moore, R.K., Fung, A.K., 1986. Microwave Remote Sensing: Active and Passive. Volume III: From Theory to Applications. 3. Artech House, Inc., Dedham, MA.
United States Department of Agriculture National Agricultural Statistics Service (USDA NASS), 2010. Field Crops Usual Planting and Harvesting Dates. USDA NASS , October. Retrieved from. http://usda.mannlib.cornell.edu/usda/current/planting/planting-10-29-2010.pdf.
USDA NASS, 2009–2012. National Agricultural Statistics Service Cropland Data Layer. Retrieved February 10, 2016, from. http://nassgeodata.gmu.edu/CropScape/.
USDA NASS, 2011. USDA, National Agricultural Statistics Service, 2010 California Cropland Data Layer Metadata. Retrieved December 19, 2016 from. https://www.nass.usda.gov/Research_and_Science/Cropland/metadata/metadata_ca10.htm.